


Molecular orientational distribution function of a chiral de Vries smectic liquid crystal from birefringence measurements

Cite as: J. Chem. Phys. **150**, 084901 (2019); <https://doi.org/10.1063/1.5080222>

Submitted: 06 November 2018 . Accepted: 11 January 2019 . Published Online: 22 February 2019

V. Swaminathan , V. P. Panov , A. Kocot , and J. K. Vij 

COLLECTIONS

 This paper was selected as Featured



View Online



Export Citation



CrossMark

ARTICLES YOU MAY BE INTERESTED IN

[eGFRD in all dimensions](#)

The Journal of Chemical Physics **150**, 054108 (2019); <https://doi.org/10.1063/1.5064867>

[Advances in the experimental exploration of water's phase diagram](#)

The Journal of Chemical Physics **150**, 060901 (2019); <https://doi.org/10.1063/1.5085163>

[Partially \(resp. fully\) reversible adsorption of monoterpenes \(resp. alkanes and cycloalkanes\) to fused silica](#)

The Journal of Chemical Physics **150**, 074701 (2019); <https://doi.org/10.1063/1.5083585>

Molecular orientational distribution function of a chiral de Vries smectic liquid crystal from birefringence measurements

Cite as: J. Chem. Phys. 150, 084901 (2019); doi: 10.1063/1.5080222

Submitted: 6 November 2018 • Accepted: 11 January 2019 •

Published Online: 22 February 2019



View Online



Export Citation



CrossMark

V. Swaminathan,¹  V. P. Panov,¹  A. Kocot,²  and J. K. Vij^{1,a)} 

AFFILIATIONS

¹Department of Electronic and Electrical Engineering, Trinity College Dublin, The University of Dublin, Dublin 2, Ireland

²Faculty of Computer Material Sciences, Institute of Technology and Mechatronics, Silesian University, Katowice, Poland

^{a)}Author to whom correspondence should be addressed: jvij@tcd.ie

ABSTRACT

An alternative method for determining the orientational distribution function and the order parameter from the electric field-induced birefringence measurements of a chiral liquid crystal compound in its Smectic A* is being introduced. A chiral mesogen based on a 5-phenyl-pyrimidine benzoate core terminated by a trisiloxane group on one side and the chiral alkyloxy chain on its opposite side is designed and synthesized to exhibit the “de Vries” smectic characteristics. The compound exhibits first order Smectic A*–Smectic C* phase transition, evidenced by the results of differential scanning calorimetry. The material is being investigated by electro-optical experiment in its smectic phases. We present a model that incorporates the generalised Langevin-Debye model which includes the Maier-Saupe effective mean-field potential term in order to explain the change in birefringence with the electric field. A good agreement between the experimental results and the predictions from the model leads to the determination of the molecular orientational distribution function in Smectic A phase. Furthermore, the temperature dependency of the Saupe orientational order parameter $\langle P_2 \rangle$ is obtained using the parameters of the model. Based on the experimental and theoretical results, we show that de Vries Smectic A* phase exhibits a broad volcano-like tilt angle distribution with the two maxima occurring at finite tilt angles closer to the Smectic A*–Smectic C* transition temperature, and a sugarloaf-like distribution occurs in the tilt for temperatures close to the Isotropic–Smectic A* phase transition.

Published under license by AIP Publishing. <https://doi.org/10.1063/1.5080222>

I. INTRODUCTION

Thermotropic liquid crystals (LCs) of calamitic molecules exhibit different smectic phases¹ in which the layered molecular arrangements are characterised with reference to the molecular long axis \mathbf{z} with respect to the layer normal \mathbf{Z} . When \mathbf{z} is parallel to \mathbf{Z} , this phase is a conventional orthogonal Smectic A (SmA). On cooling the sample, this phase is followed usually by a tilted Smectic C (SmC), in which the axis \mathbf{z} is tilted by angle θ with respect to the layer normal, \mathbf{Z} (Fig. 2).^{1,2} When the molecules are chiral, these phases are denoted by SmA* and SmC*. The transition from the SmA* to SmC* phase on cooling is associated with the emergence of the molecular tilt angle θ with respect to \mathbf{Z} . The angle θ can be as large as 45°, leading to layer shrinkage² as high as ~29%. The combined

effect of layer shrinkage with a reduction in temperature and the surface anchoring of liquid crystalline molecules results in buckling of the smectic layers, leading to the formation of chevron structure/s.³ The opposite folds of the chevron structures form a void in the middle of these folds with the result that zigzag line defects in the texture are exhibited. These in turn reduce the contrast ratio due to severe degradation of the optical quality of Ferroelectric Liquid Crystal (FLC) displays⁴ which is brought about by the chevron structure. One of the plausible solutions to overcome this limitation is to develop a FLC material with minimal or ideally zero layer-shrinkage.²

Diele *et al.*⁵ were the first to report a number of smectic LCs to have the layer thickness (d) lower than the molecular length (l) in the SmA phase. De Vries⁶ studied one of these

compounds that showed no significant change in the layer thickness, d , at the SmA to SmC transition. Based on the experimental results, de Vries suggested that molecules are already tilted in the SmA phase and a long-range molecular correlation in the tilt direction is attained in each layer at the transition temperature. However the tilt direction, i.e., the azimuthal angle of this tilt varies randomly from layer to layer in a manner that the SmA phase itself is uniaxial. Later, Leadbetter and Norris⁷ reported a low orientational order parameter ($\langle P_2 \rangle$) of the SmA phase of a compound, synthesized by George Gray's group in Hull, UK, using X-ray diffraction studies and they also obtained a broad orientational molecular distribution function. Following the availability of these experimental results, de Vries proposed a second model⁸⁻¹⁰ where he suggested that molecules are tilted in the SmA phase with only a short-range correlation in the direction of the tilt; however the azimuthal angle varies spatially even within a single smectic layer. This also leads to uniaxial SmA phase. In addition to it, de Vries found that these materials exhibit the first order SmA-SmC phase transition in contrast to the usual second order displayed by conventional smectics. The materials that show such unique characteristics have recently been designated as "de Vries smectics."

Subsequent experimental works on chiral de Vries smectics revealed additional interesting properties, some of which are listed below:

1. A large electro-clinic co-efficient.^{11,12}
2. A decrease in the birefringence with a reduction in temperature in the SmA* phase.
3. A large field-induced increase in the birefringence in the SmA* phase especially close to the SmA*-SmC* transition temperature.¹³⁻¹⁵
4. A non-monotonic trend in the layer thickness and the birefringence both as a function of temperature and electric field.¹⁴⁻²⁰
5. The absence of nematic phase in these materials.^{2,21}

Clark *et al.*²² explained the electro-clinic effect (ECE) of de Vries smectics by assuming that the molecules have a fixed cone angle θ_A , with the proviso that $\theta_A \neq 0$. The molecules are distributed over the cone in the Langevin-Debye model [Fig. 1(a)]. This model was modified by Shen *et al.*,²³ who termed it the generalised Langevin-Debye model. They altered the original model to better explain the de Vries characteristics of a change in the (i) birefringence and (ii) apparent tilt angle, with applied electric field. A representative distribution function $f(\theta)$ for these two models is shown in Figs. 1(a) and 1(b), respectively. In the Langevin-Debye model,²² the tilt distribution is maximum at a finite angle [shown $\theta_A = 20^\circ$ as on example, Fig. 1(a)]. In the generalised Langevin-Debye model,²³ the angles for which the maxima in the orientational distribution function (ODF) lie within the range of the maximum and the

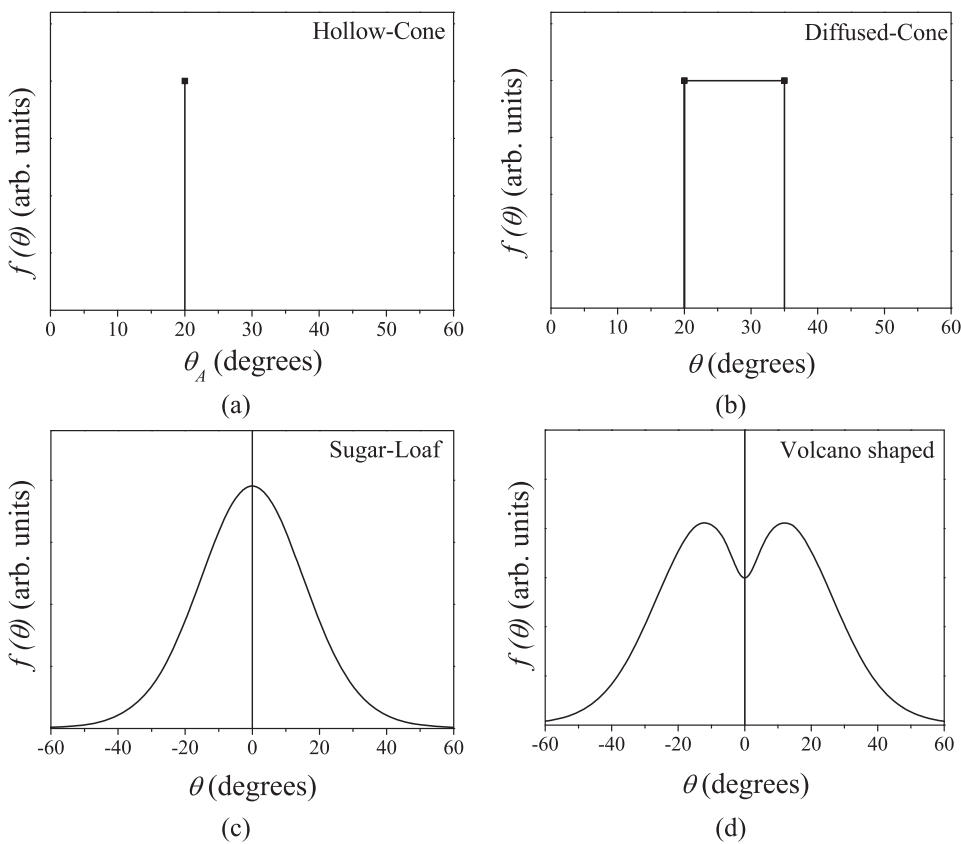


FIG. 1. The schematic plots that represent different orientational distributions of the tilt angle θ of the molecular long axis with respect to the layer normal of the de Vries SmA phase: (a) hollow-cone (fixed angle θ_A), (b) diffused-cone, (c) sugarloaf, and (d) volcano-shaped.

minimum values of θ . These limits depend on (i) the magnitude of zero-field birefringence and (ii) the birefringence for a maximum field applied across a planar-aligned cell. These models can be called “hallow cone” and “diffused-cone,” and a detailed description of the models is given in [Appendices A and B](#). The other plausible tilt distribution functions used in this context correspond to the “sugar-loaf” and “volcano-shaped” distributions;^{24–28} the plots of which are given in [Figs. 1\(c\) and 1\(d\)](#), respectively. The hollow and the diffused-cone distribution functions are the two extreme examples of the volcano-shaped distribution function.

This article reports the studies of a newly designed and synthesized chiral smectic LC for this work. The experimental results of the birefringence of the cell as a function temperature and electric field are obtained on planar-aligned cells of this compound. The results show that the investigated chiral smectic compound displays the entire features of a de Vries smectic liquid crystalline. In this article, we present a new electro-optic (EO) model that combines the mean-field potential of the generalised Langevin–Debye model with the addition of a modified expression from the Maier–Saupe mean-field theory. The proposed model is used to obtain the ODF; this leads us to determination of the orientational order parameter $\langle P_2 \rangle$ from the results of the electric field induced birefringence measurements.

II. THEORY

Garoff and Meyer²⁹ showed that the tilt of the molecular director \vec{n} with respect to the layer normal \mathbf{Z} can be induced in the SmA^* phase by applying an electric field parallel to the smectic layers. This is known as the electro-clinic effect (ECE). In a planar-aligned liquid crystalline cell, the average induced tilt results in a tilt of the optical axis, θ_{ind} , with respect to the layer normal as “distribution of the molecular directors” are altered by the field. The field-induced director redistribution manifests itself into a change of the birefringence. The electro-optic response in this context implies observations of both θ_{ind} and Δn , as a function of the applied electric field. The conventional FLCs show a linear EO response in the SmA^* phase. By contrast, the de Vries smectics show a pronounced change both in θ_{ind} and Δn with applied field and also gives rise to a characteristic sigmoidal shaped EO response, especially, close to the SmA^* – SmC^* transition temperature.

A theoretical approach to EO modelling starts from the use of an effective mean-field potential of the generalised Langevin–Debye model²³ to which a modified Maier–Saupe distribution⁹ term of effective potential is added. Hence the effective mean-field potential U of the proposed model is written as follows:

$$U = -A^2 \cos^2(\theta - \theta_0) - p_0 E \sin \theta \cos \phi (1 + \alpha E \cos \phi). \quad (1)$$

Angles θ and ϕ are defined in the laboratory frame and shown in [Fig. 2](#). Here $p_0 \sin \theta$ is magnitude of dipole moment of a domain in which the tilt directions are correlated with each other. The linear term in \mathbf{E} expresses the interaction of the

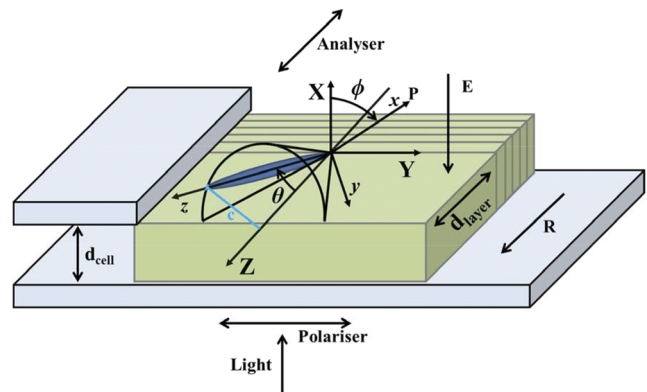


FIG. 2. A schematic representation of the EO geometry of a planar-aligned cell. \mathbf{X} , \mathbf{Y} , and \mathbf{Z} and \mathbf{x} , \mathbf{y} , and \mathbf{z} are the laboratory and the molecular frames of references, respectively. The LC material is sandwiched in between the two ITO-deposited glass plates of cell thickness (d_{cell}). The molecular long axis \mathbf{z} is tilted by an angle θ from the layer normal \mathbf{Z} . The \mathbf{c} director (shown as a blue line) is the projection of the molecular long axis on the smectic-layer plane where the induced polarization \mathbf{P} is normal to the \mathbf{c} director. \mathbf{P} makes an angle ϕ with the axis directed normal to the substrate as \mathbf{X} . An electric field \mathbf{E} applied across the cell is parallel to the smectic-layers. This brings about a change in the intensity of the transmitted light between the crossed polarizers by the field, with the light incident normally to the cell.

dipole moment of this domain with the field. The quadratic term in \mathbf{E} and its scaling factor α give rise to the tilt susceptibility for higher amplitudes of the electric field. This term is representative of the energy stored in the dielectric. On the level of a single molecule, this term involves coupling between the magnitude of electric field and the additional molecular dipole moment induced by the field; hence, the model parameter α may be related to the polarizability anisotropy. This term also leads to a sigmoidal response of the birefringence to the applied field. The electric field independent expression $A^2 \cos^2(\theta - \theta_0)$ is the mean-field potential term responsible for restoring the constituent molecules to a minimum packing entropy of the system. θ_0 is one of the model parameters that defines the maximum probable molecular long axis tilt with respect to the layer normal in the absence of electric field.

The coefficient of Legendre-polynomial for $n = 2$, P_2 , of a uniaxial liquid crystalline phase is given as

$$P_2 = \frac{1}{2}(3\cos^2\theta - 1). \quad (2)$$

The Saupe orientational order parameter in the laboratory frame with the mutually perpendicular axes: \mathbf{X} , \mathbf{Y} , and \mathbf{Z} can be calculated by averaging the corresponding Legendre-polynomial coefficient multiplied with the ODF as follows:

$$\langle x \rangle = \int_0^{\frac{\pi}{2}} \int_0^{2\pi} x(\theta, \phi) f(\theta, \phi) \sin \theta d\theta d\phi, \quad (3)$$

where $\langle x \rangle$ denotes an ensemble average of “ x ” (i.e., $\langle x \rangle = \langle P_2 \rangle$). The mean-field molecular ODF $f(\theta, \phi)$ is defined as follows:

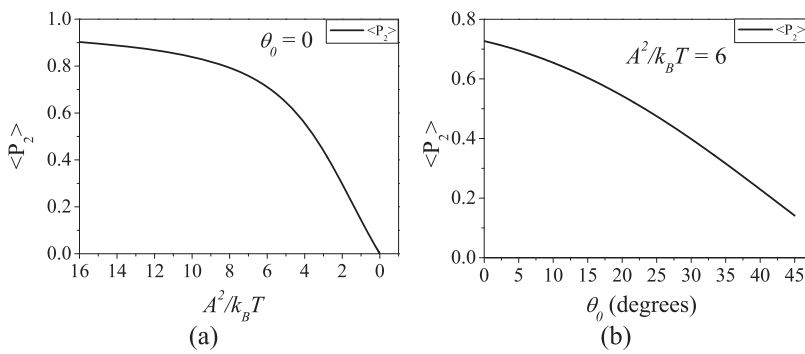


FIG. 3. The relationship between (a) the orientational order parameter and $(A^2/k_B T)$ for the sugarloaf-like molecular distribution and (b) the orientational order parameter is plotted versus θ_0 , for a fixed value of $(A^2/k_B T)$. Both curves are the plots for the electric field equal to zero. θ_0 is defined in the text.

$$f(\theta, \phi) = \exp[-U/k_B T] / \int_0^{\pi/2} \int_0^{2\pi} \exp[-U/k_B T] \sin \theta d\theta d\phi. \quad (4)$$

U from Eq. (1) is inserted in Eq. (4), and the ODF $f(\theta, \phi)$ is numerically calculated with the limits of θ_{\min} and θ_{\max} extended from 0 to $\pi/2$. The term $(A^2/k_B T)$ describes the molecular tilt fluctuations; the width of ODF decreases as the value of $(A^2/k_B T)$ increases. Wider the ODF, lower the order parameter and vice versa. These results are evidenced by the plot in Fig. 3(a). The angle θ_0 defines the shape of the ODF (Fig. 4). For $\theta_0 < (k_B T/A^2)$, the sugarloaf-like distribution (the Gaussian distribution) is obtained, whereas for $\theta_0 > (k_B T/A^2)$ the volcano-shaped distribution function is obtained. Here $2\theta_0$ is the “aperture angle” of the volcano-shaped distribution function.

On neglecting the molecular biaxiality of liquid crystalline molecules and on averaging the dielectric tensor over the ODF, Shen *et al.* derived an expression for the birefringence that is normalised by the maximum birefringence²³ as follows:

$$\frac{\Delta n}{\Delta n_{\max}} = \frac{\langle \cos^2 \theta - \sin^2 \theta \cos^2 \phi \rangle}{\cos 2 \left(\frac{1}{2} \tan^{-1} \left(\frac{\langle \sin 2\theta \cos \phi \rangle}{\langle \cos^2 \theta - \sin^2 \theta \cos^2 \phi \rangle} \right) \right)}. \quad (5)$$

Here Δn is the measured birefringence of the LC compound in the planar-aligned cell and Δn_{\max} is the saturated birefringence at a temperature well within the SmC* phase for the maximum field applied across a planar-aligned cell. Various averages in Eq. (5) are estimated by using Eq. (3) which is the standard procedure.

The order parameter is simulated using Eqs. (3) and (4) for the zero electric field across the cell (i.e., $E = 0$ thus p_0 and α do not play any role in the calculation of the order parameter). The field-induced birefringence is simulated using Eq. (5) and fitted to the experimental data with the objective of determining the effect of θ_0 on the value of the order parameters calculated in our model.

The term $(A^2/k_B T)$ describes the mean-field nematic interaction energy compared to the thermal energy. A higher value of $(A^2/k_B T)$ implies a “larger molecular interaction energy.” These are clearly evident from the large values of the orientational order parameter shown in Fig. 3(a) for various values of $(A^2/k_B T)$. Figure 3(b) shows a relationship between the orientational order parameters and θ_0 , plotted for a fixed value of $(A^2/k_B T)$. We find that for $\theta_0 = 0^\circ$, the order parameter attains the maximum value. The simulation results do

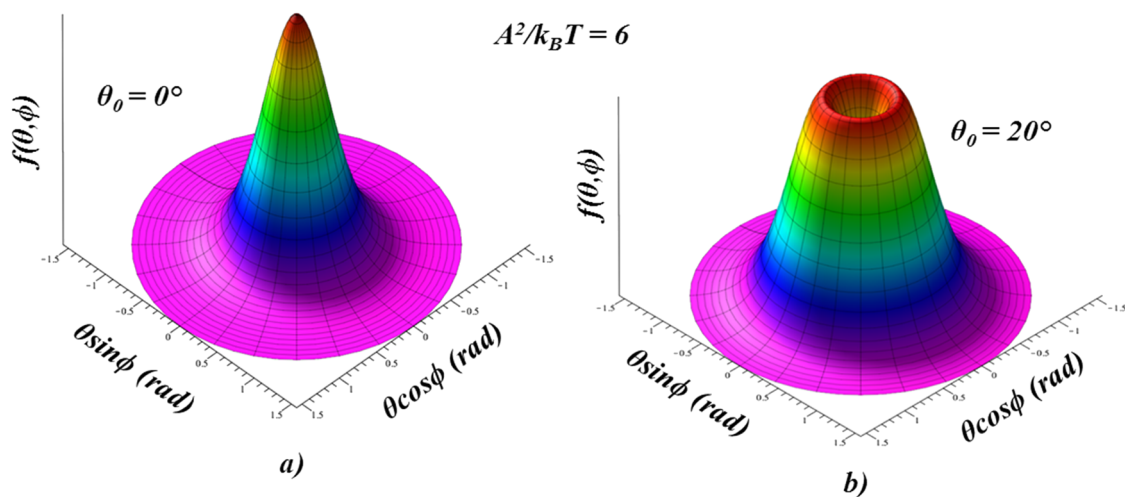


FIG. 4. The effect of θ_0 on the shape of the distribution function and a 3-D representation of the ODF (a) for $\theta_0 = 0^\circ$ and (b) for $\theta_0 = 20^\circ$, and in both cases, $A^2/k_B T$ is fixed.

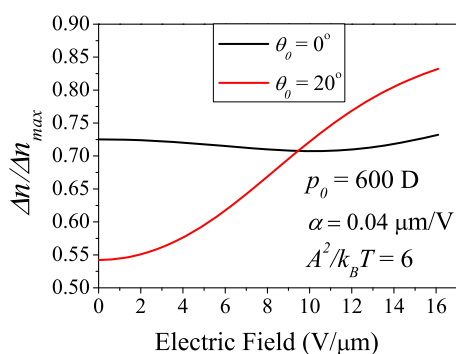


FIG. 5. The simulated electric-field induced for two values of θ_0 on the shape of the birefringence curves. The parameters p_0 , α , and $(A^2/k_B T)$ are fixed. The red curve is realistic. If $(A^2/k_B T) = 5$, the birefringence plot is similar to the black line but the zero field birefringence is reduced.

show that if $\theta_0 \neq 0^\circ$, the order parameter is low as observed experimentally⁷ for the de Vries smectics.

In Fig. 5, if $\theta_0 = 0^\circ$, then the ODF is sugarloaf-like. In that case, we surprisingly find that $\Delta n/\Delta n_{\max}$ hardly changes with E (black line). This is also true; if $(A^2/k_B T)$ is reduced, the zero field birefringence will also be reduced. From this model, we find that we need a finite value of θ_0 in order for the birefringence can vary with the field as is experimentally observed. Since the experimental results^{23,30} follow the simulated birefringence curve as shown in Fig. 5 (red line), we can safely conclude that for a set of realistic chosen values for p_0 , α , and $(A^2/k_B T)$, the volcano-like distribution is the clear outcome from these investigations.

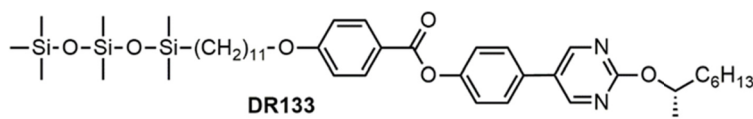
An approach involving the three-parameter model has recently been used by Sreenilayam *et al.*³¹ to fit the apparent optical tilt angle as a function of the electric field of a de Vries smectic material. In that model, the effective potential involved a linear term in the field and the distribution term as used here. This model developed earlier by us³¹ was termed

“the three parameters mean-field model” involving parameters A , p_0 , and θ_0 . However, there are a number of limitations of that model. The main limitation being that it cannot be used to fit the birefringence data of a de Vries smectic mainly due to the absence of the quadratic term in the electric field. Secondly, the ODF has been found to be surprisingly narrow in the distribution of tilt angle. This therefore requires further investigations as are being attempted here to carry out a critical appraisal of the fitting of the electro-optic properties especially the electric-field induced birefringence as a function of the applied field of de Vries smectics.

III. EXPERIMENT

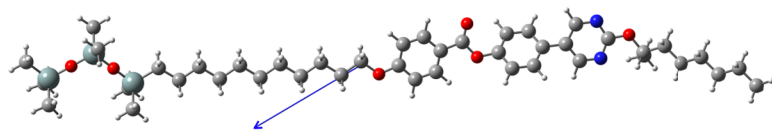
The compound DR133 is based on using the 5-biphenylpyrimidine benzoate core, terminated on one side by trisiloxane and on the opposite the core is attached to the chiral alkyloxy chain. Details of the synthesis will be given elsewhere. Siloxane termination promotes lamellar orderings, leading to a well-defined layer structure and the exhibition of de Vries smectic-like behaviour^{21,32} in the SmA phase. A strong layering prevents formation of the nematic phase in the known phase sequence. The molecular structure and the transition temperatures with the enthalpies of transition given in the square brackets for DR133, on cooling, are given in Fig. 6(a).

The nature of the phase transitions and the transition temperatures are investigated using Perkin-Elmer DSC-7 differential scanning calorimetry (DSC) while the sample is cooled at the rate of $10^\circ\text{C min}^{-1}$ (DSC thermogram is shown in Appendix E). An optimized geometry of DR133 [Fig. 6(b)] is obtained by the Density Functional Theory (DFT) using the B3LYP method and the 6-31G (d,p) level of the basis set. The optimized geometric computations are carried out using a Gaussian 09 software package.³³ The molecular length of DR133 is estimated to be $\sim 42 \text{ \AA}$, and the dipole moment is calculated as $\mu = 5.8 \text{ D}$.



(a)

Cr 31°C [41.41 Jg^{-1}] SmC* 94°C [0.97 Jg^{-1}] SmA* 102°C [4.04 Jg^{-1}] Iso



(b)

FIG. 6. (a) The molecular structure of the compound DR133; the phase sequence and the transition temperatures on cooling, ($T/^\circ\text{C}$), with the transition enthalpies ($\Delta H/\text{Jg}^{-1}$) are determined from DSC (b) The optimized molecular geometry of DR133 is shown. The arrow pointing outwards in (b) shows the direction of the molecular dipole moment, $\mu = 5.8 \text{ D}$; Iso and Cr stand for the isotropic and crystalline states, respectively.

The birefringence Δn is measured using an automated technique of time-resolved polarimetry (ATP) developed in our laboratory. The basic principle of the method was given by Park *et al.*³⁴ The experimental setup for the ATP includes the Polarizing Optical Microscope (POM), in which the polarizer and the analyzer can separately and independently rotated automatically. The intensity of the transmitted light (Red LED wavelength $\lambda = 633$ nm) passing through a LC sample is recorded using a 16-bit data acquisition board (Keithley® KUSB-3116). A triangular wave electric field signal is applied across the planar-aligned sample. The procedure starts by fixing the polarizer position (α_P) with respect to the reference direction and then acquiring transmitted intensity (a dataset corresponding to one cycle of the applied voltage waveform) for at least 3 different positions of the analyzer (α_A). At the given instant of time, the intensity, $I(\alpha_A)$, as a function of the position of the analyzer is given by a sine wave function with the bias B , amplitude $(S^2 + C^2)^{\frac{1}{2}}$, and an initial phase angle of $\tan^{-1}(C/S)$:

$$I(\alpha_A) = I_0(S \sin 2\alpha_A + C \cos 2\alpha_A + B). \quad (6)$$

Here I_0 is the intensity of the light source. The coefficients S , C , and B , are biased sine wave functions of the polarizer position α_P as given below

$$S = S_S \sin 2\alpha_P + C_S \cos 2\alpha_P + B_S, \quad (7)$$

$$C = S_C \sin 2\alpha_P + C_C \cos 2\alpha_P + B_C, \quad (8)$$

$$B = S_B \sin 2\alpha_P + C_B \cos 2\alpha_P + B_B. \quad (9)$$

Therefore, by repeating the above procedure for at least three different positions of the polarizer, α_P , we can obtain the desired nine coefficients (S_S , C_S , B_S , S_C , C_C , B_C , S_B , C_B , and B_B) by fitting the recorded data to Eqs. (6)–(9). The experimental error can be reduced by increasing the number of polarizer/analyzer positions used in the data acquisition experiment. Note that this will not require any changes to the algorithm of the data processing. On assuming that a liquid crystalline cell can be represented by a uniform retardation plate of the magnitude, $\Delta n d_{\text{cell}}$, we can relate the retardation value to the coefficients using either the Jones or the Mueller matrix³⁵

$$\cos\left(\frac{\pi \Delta n d_{\text{cell}}}{\lambda}\right) = \sqrt{\frac{C_C + S_S}{2B_B}}. \quad (10)$$

Since the signal applied to the sample is periodic (triangular wave used in most experiments), the response to the applied waveform can be acquired sequentially for each set of the polarizer/analyzer position. Therefore, we can obtain these nine coefficients for every point on the waveform (a sample dataset for selected points from the experiment is given in Appendix D). Thus the real-time response of the birefringence to an applied electric field can be measured.

The layer thickness in both SmA* and SmC* was measured using X-ray diffraction; the maximum layer shrinkage of this compound, relative to the thickness at the SmA* to SmC* transition temperature, has been found to be 1.7% in the SmC* phase. The details will be published elsewhere.

IV. RESULTS AND DISCUSSIONS

The thickness of a planar-aligned liquid crystalline cell is calculated from the interference fringes for the cell as $1.9 \mu\text{m}$. A triangular wave electric field of amplitude $20 \text{ V}_{0\text{-pk}}/\mu\text{m}$ and $f = 224$ Hz is applied across the cell. Frequency of the signal is optimized to avoid hysteresis in the observed response as it happens for very low frequencies, and it also minimizes the response of conductivity due to ionic effects (reduced by increasing the frequency of the probe field). The frequency is low enough to allow for a sufficient time for the electro-optic switching to completely occur and is large enough so that the ions cannot follow the alternating field. Figure 7 shows the temperature dependence of Δn for zero (Δn_0) and large fields (Δn_E , $E = 20 \text{ V}/\mu\text{m}$); Δn_0 surprisingly decreases in the SmA* phase on cooling from the isotropic state towards the SmA*–SmC* transition temperature and is observed to reach a minimum value at the SmA*–SmC* phase transition temperature T_{AC} .

Normally, the birefringence should have increased as a result of an increase in the orientational order parameter with a reduction in temperature. Hence an anomalous decrease in Δn_0 indicates an emergence of the molecular tilt angle where the azimuthal angle ϕ of the molecular directors is distributed around the cone for maintaining uniaxiality of the SmA* phase. Since the molecular distribution is spatially averaged in the optical experiment, the effective value of birefringence decreases. On applying the electric field across a planar-aligned cell, the birefringence Δn_E does not change with the field close to the isotropic–SmA* transition temperature. However on approaching $T = (T_{AC} + 3)^\circ\text{C}$, we observe a significant increase in Δn_E with the field. On further cooling, Δn_E diverges to become 30% higher than Δn_0 at $T = T_{AC}$ by the electric field. This implies that in close proximity to T_{AC} , applied electric field lifts degeneracy in azimuthal angle ϕ while the molecular directors are redistributed by the field (field dependent Δn data for a few selected temperatures are shown in Appendix C to highlight the basic differences

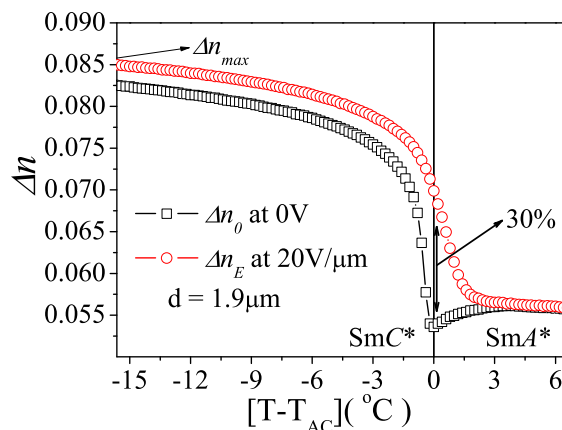


FIG. 7. The temperature dependence of Δn for zero (\square) and $20 \text{ V}/\mu\text{m}$ [red circle] applied electric fields.



FIG. 8. The textures are recorded by POM under crossed polarizers on a planar-aligned cell of thickness $9\ \mu\text{m}$ filled with DR133 at a temperature of $(T_{AC} + 1)\ ^\circ\text{C}$ in the SmA^* phase for different strengths of the applied electric field. T_{AC} is the SmA^* to SmC^* transition temperature. The double headed arrow represents the rubbing direction in the cell. A large increase in the field-induced birefringence is recorded as typical texture for de Vries Smectic.

between SmA^* and SmC^* phase). A change in the interference colors is observed as a function of the applied electric field (see Fig. 8). Such a significant change in the birefringence/interference colors with electric field is a signature of the de Vries smectics (Fig. 9).²⁰

Plots of Δn normalised by its maximum value are shown in Fig. 9 as a function of the electric field for different temperatures. The experimental data (presented as symbols) are fitted to the model expressed in terms of Eq. (5). Fits of the data to the model are shown by the solid lines. We note that $\Delta n/\Delta n_{max}$ linearly increases with electric field at higher temperatures in the SmA^* phase, i.e., particularly closer to the Iso- SmA^* transition temperatures. While on cooling the sample, the electric field saturates Δn as well as leads to a sigmoidal-shaped response, seen here for $T \leq (T_{AC} + 1.8)\ ^\circ\text{C}$.

The temperature dependent variations of the fitting parameters are shown in Fig. 10. The local dipole moment p_0 diverges [Fig. 10(a)] on approaching the SmA^* - SmC^* phase transition temperature; the divergence in p_0 corresponds to an increase in the size of the tilt-correlated domain. The scaling parameter α gives the strength to the quadratic term in the field; this increases almost linearly on cooling from the

Iso- SmA^* phase transition temperature [Fig. 10(b)]. This trend is altered at $T \sim (T_{AC} + 1.5)\ ^\circ\text{C}$, where the birefringence saturates for low values of the electric field. Both $(A^2/k_B T)$ [Fig. 10(c)] and the aperture angle $2\theta_0$ [Fig. 10(d)] diverge with a reduction in temperature as T approaches T_{AC} . It is surprising to note that the parameter α is close to zero at the SmA^* to SmC^* transition temperature. However $p_0\alpha$ needs to be compared with A^2 . We find from Fig. 10(c) that the factor $\frac{A^2}{k_B T}$ increases from 6 to 17; an almost 3 fold increase is observed. This is mainly due to an increase in A^2 on a reduction in temperature (T appears in the denominator, but the percentage decrease in T is not so-large over a given range of temperatures). On the other-hand, the product $p_0\alpha$, see Figs. 10(a) and 10(b), decreases by a similar factor. Hence the decrease in the parameter α in the model may possibly be due to the relative dominance of the term in A^2 relative to that of $p_0\alpha$. θ_0 may also play a dominant role at the cross-over temperature, which in this case is approximately $1.5\ ^\circ\text{C}$ above the SmA^* to SmC^* transition temperature.

De Gennes suggested that anisotropy in a physical quantity of a liquid crystal is an indirect measure of its orientational order parameter, i.e., $\langle P_2 \rangle$.³⁶ The ratio between the anisotropy in its free state, δG (where $\delta G = G_{\parallel} - G_{\perp}$), and the anisotropy in the perfect ordered state (ΔG) can give us the macroscopic orientational order parameter ($S = \langle P_2 \rangle = \delta G/\Delta G$). This approach is used for estimating S from measurements of the anisotropy in the dielectric permittivity and the optical refractive indices.³⁷⁻³⁹ In this work, we use the following concept: Δn_{max} is the maximum value of saturated optical anisotropy for a perfect ordered system; ratio $\Delta n/\Delta n_{max}$ provides for a rough estimation of the order parameter $\langle P_2 \rangle$. Therefore, we use values of the fitting parameters from the mean-field modelling, namely, $(A^2/k_B T)$ and θ_0 to extract the Saupe orientational order parameter in the laboratory frame. Note that these parameters provide the tilt distribution of the molecular long axis in the absence of the electric field (Fig. 11).

Several techniques such as NMR,⁴⁰ X-ray scattering,⁴¹ Raman,⁴² and infrared spectroscopies⁴³ are used to obtain the orientational order parameters of different de Vries smectics and most of these works are published in the literature. The Raman and IR spectroscopic measurements on a prototypical de Vries smectic TSiKN65 led to $\langle P_2 \rangle = \sim 0.4$.⁴³ This value is found to be rather low in magnitude for the SmA^*

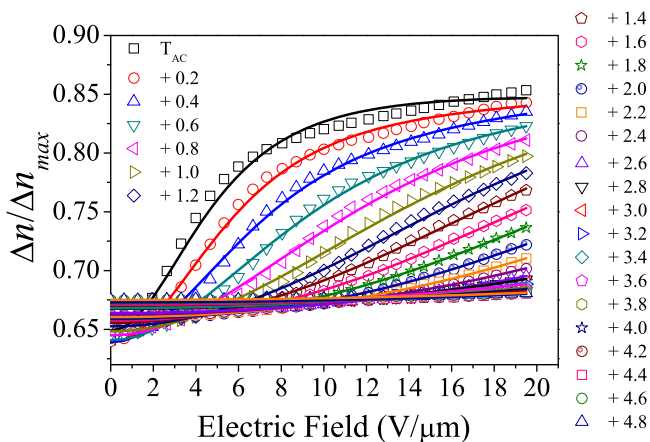


FIG. 9. The plots of normalized birefringence $\Delta n/\Delta n_{max}$ as a function of the electric field. The field is applied across a planar-aligned cell for a range of temperatures in the SmA^* phase. $\Delta n_{max} = 0.085$ is taken from Fig. 8 as shown there. The symbols represent the experimental data, and the solid lines are fits to the model.

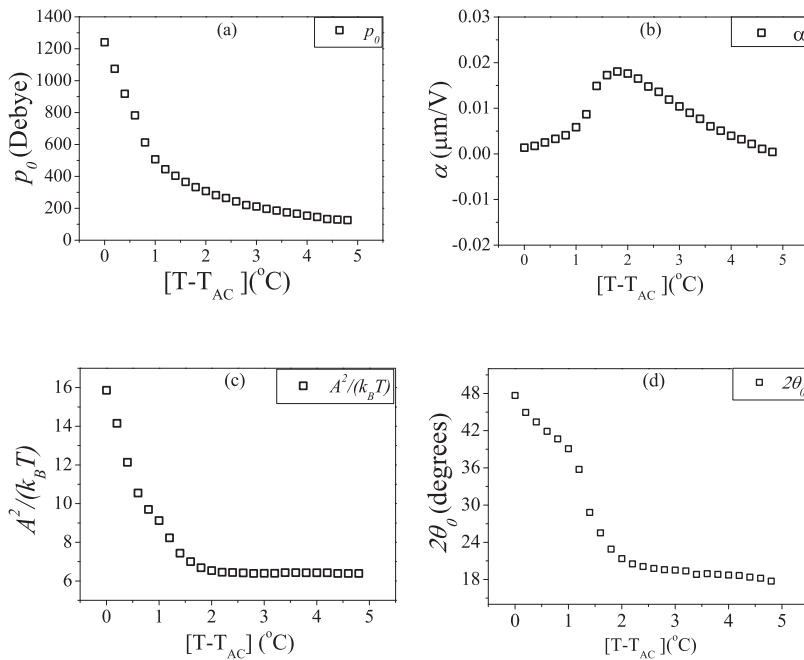


FIG. 10. Temperature dependencies of the fitting parameters: (a) the local dipole moment p_0 , (b) the scaling factor α for the quadratic term, (c) $A^2/k_B T$, and (d) $2\theta_0$ is the aperture angle.

phase. However, NMR, Raman, and the X-ray spectroscopic investigations of another low layer-shrinkage smectic 9HL compound yielded $\langle P_2 \rangle$ as large as ~ 0.8 , this value was determined over a wide temperature range of the SmA^* phase.⁴⁴ The X-ray studies of two achiral de Vries smectics C4 and C9 gave $\langle P_2 \rangle \sim 0.6$.²⁸ Values of $\langle P_2 \rangle$ greater than 0.6 lead to sugarloaf ODF in the SmA phase, whereas for low $\langle P_2 \rangle$ it led to the volcano-shaped ODF. At the same time, a large electro-clinic coefficient is exhibited by these compounds.

For the DR133 material investigated here, $\langle P_2 \rangle \sim 0.67$ close to the Iso- SmA^* transition temperature and it decreases to ~ 0.63 close to the $\text{SmA}^*-\text{SmC}^*$ phase transition temperature as a direct result of the broadening of the ODF in the tilt angle [this leads to a large value of the aperture angle, Fig. 10(d)]. The

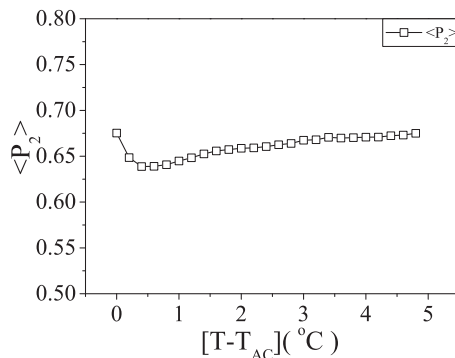


FIG. 11. The temperature dependence of the orientational order parameter, $\langle P_2 \rangle$.

observed $\langle P_2 \rangle$ for this smectic material is not found to be as low as for TSiKN65 but is also not as high as ~ 0.8 for a conventional smectic A phase.

Figure 12 shows the ODF $f(\theta, \phi)$, at a temperature of $(T_{AC} + 1)^{\circ}\text{C}$, for different magnitudes of the electric field. This is a projection of the 3-D ODF onto a plane normal to the $\theta \cos \phi$ axis (Fig. 4). At zero electric field (line in black) the molecules are evenly distributed with the maximum probability coinciding at a finite angle ($\sim 20^{\circ}$) with respect to the layer normal.

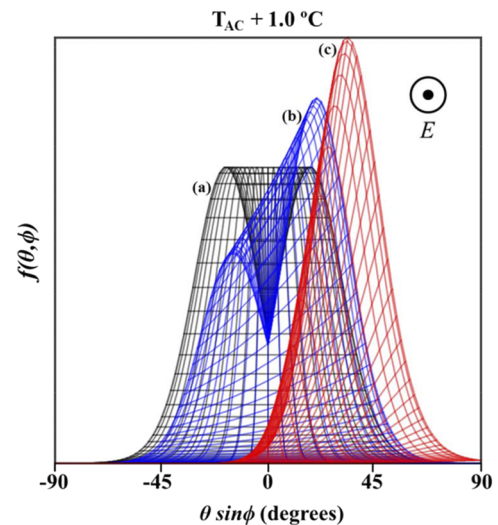


FIG. 12. The orientational distribution function $f(\theta, \phi)$ of DR133 for $(T_{AC} + 1)^{\circ}\text{C}$ for different electric fields (a) 0 $\text{V}/\mu\text{m}$, (b) 2 $\text{V}/\mu\text{m}$, and (c) 20 $\text{V}/\mu\text{m}$.

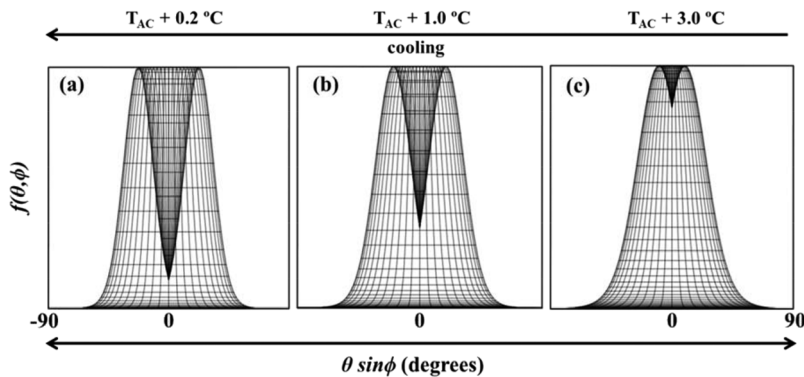


FIG. 13. Temperature dependent change in the ODF for selected temperatures close to the smectic A to C transition (a) ($T_{AC} + 0.2$ °C), (b) ($T_{AC} + 1$) °C, and (c) ($T_{AC} + 3$) °C at zero electric field.

On applying the electric field, the molecules shift towards the favourable direction than in the opposite direction. Similar results have been given by Kocot *et al.*⁴⁵ for a de Vries smectic by Raman spectroscopy. For higher amplitudes of the electric field, the distribution gets condensed to a narrow range of ϕ values leading to single maxima in the ODF.

Figure 13 shows ODF for different temperatures. It is obvious that for temperatures close to the Iso-SmA* phase transition temperature [Fig. 13(c)], the distribution can be described by a single Gaussian function (i.e., Sugarloaf-like distribution); satisfactorily, the observed small drop in the magnitude of the function at zero degree is due to a limitation in the model; however a drop in the ODF is negligibly small. On cooling the sample, it is evident that drop in the magnitude increases and the distribution function splits into two separate Gaussian functions (i.e., volcano-shaped). This is observed at a temperature of ~ 2 °C below the Iso-SmA* transition temperature, where the contribution of θ_0 overtakes that of $A^2/R_B T$ (Fig. 14). All these factors emphasise the presence of a wider split in the two maxima of the ODF as shown in Fig. 13(a). Similar conclusions have been made for other de Vries smectic liquid crystals, results reported in Refs. 44 and 46.

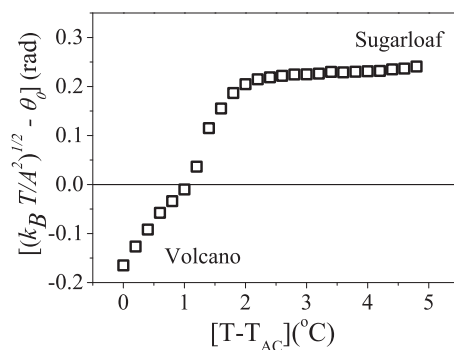


FIG. 14. The difference between $(k_B T/A^2)^{1/2}$ and θ_0 is plotted as a function of the reduced temperature depicting the cross over between Sugarloaf and Volcano-like distribution in the SmA* temperature range.

V. CONCLUSION

A new chiral LC material DR133 is shown to exhibit first order SmA*-SmC* phase transition from the results of DSC and the EO response measurements. By introducing the modified Maier-Saupe mean-field term to the generalised Langevin-Debye mean field potential expression, a good fit of this model to the experimentally measured birefringence data as a function of the applied electric field allows us to obtain the fitting parameters $A^2/R_B T$ and θ_0 , responsible for the molecular tilt distribution in the absence of electric field. These in turn allow us to estimate the Saupe orientational order parameter, $\langle P_2 \rangle$. The magnitude of $\langle P_2 \rangle$ is low for this material than for conventional smectics due to a non-zero value of θ_0 as expected for de Vries smectics. These high resolution experimental studies of birefringence in SmA* and SmC* phases of a de Vries type LC and theoretical investigations as carried out here reveal that the smectic material exhibits both sugarloaf and volcano-shaped distribution function close to the SmA*-Iso and SmA*-SmC* transition temperatures, respectively, in the temperature range of the SmA* phase. The crossover between the sugarloaf and volcano distributions appears at ~ 1.5 °C above the T_{AC} (Fig. 14).

ACKNOWLEDGMENTS

This work was supported by 13/US/I2866 from the Science Foundation Ireland as part of the U.S.-Ireland Research and Development Partnership program jointly administered with the United States National Science Foundation under Grant No. NSF-DMR-1410649. We thank Professor Satyendra Kumar for co-ordinating the project. J.K.V. thanks W. Dowling for co-supervising the work of V.S.

APPENDIX A: LANGEVIN-DEBYE MODEL

In order to explain the unusual electro-optic response observed in materials exhibiting the de Vries SmA* phase, Clark *et al.* proposed a model²² which assumes that under zero influence of an external electric field the molecules are randomly distributed over a cone with a fixed tilt angle θ_A . However, under applied electric field E the local dipole moment p

couples with ϕ , which is described by the effective mean-field potential,

$$U = -pE \cos \phi. \quad (\text{A1})$$

Although this model could reproduce many qualitative features of de Vries electro-optic response, it could not reproduce the characteristic sigmoidal shape of the observed birefringence with field.

APPENDIX B: GENERALISED LANGEVIN-DEBYE MODEL

Later, Shen *et al.*²³ modified the original model²² allowing the molecules to have degrees of freedom in both the azimuthal angle ϕ and the tilt angle θ under applied electric field. The effective mean-field potential of the generalised Langevin-Debye model is expressed as

$$U = -p_0 E \sin \theta \cos \phi (1 + \alpha E \cos \phi), \quad (\text{B1})$$

where $p_0 \sin \theta$ is the magnitude of the dipole moment of the tilt correlated domain, α is the phenomenological scaling parameter that gives the sigmoidal response in the birefringence with the applied electric field. The experimentally measured apparent tilt angle and the birefringence are fitted using the above mean-field potential expression in the free energy with the defined orientation distribution function. The average of a physical parameter $\langle x \rangle$ in the generalised Langevin-Debye model is evaluated as given below,

$$\langle x \rangle = \int_{\theta_{\min}}^{\theta_{\max}} \int_0^{2\pi} x(\theta, \phi) f(\theta, \phi) \sin \theta d\theta d\phi.$$

Here the molecules are allowed to vary in the tilt angle θ over a limited range, and the range is estimated from the experiment. θ_{\max} corresponds to the experimentally observed maximum apparent tilt angle with large enough electric field that is sufficient to saturate the response, and θ_{\min} is estimated from the measured zero field birefringence. This generalisation in the Langevin-Debye model dramatically improves the theoretical fit to the experimental data. Swaminathan *et al.*⁴⁷ recently modified this model where they replaced θ_{\min} by an angle dependent on temperature. It is found that this change better fits the experimental results on the birefringence and the apparent tilt angle of a de Vries smectic.

APPENDIX C: A COMPARISON OF THE DEPENDENCE OF Δn ON ELECTRIC FIELD IN SmA* AND SmC* PHASES

The response in terms of the dependence of Δn on E exhibits distinct differences in the SmA* and SmC* phases, see

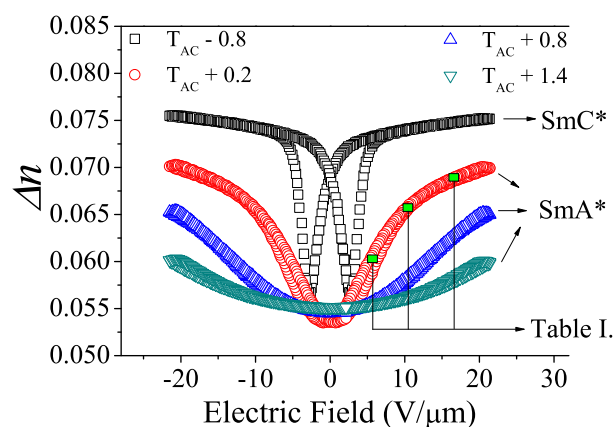


FIG. 15. The electric field dependence of Δn for a range of positive and negative values of applied electric field. We observe hysteresis for $(T = T_{AC} - 0.8)^\circ\text{C}$ (black squares), typical of SmC* phase ($f = 224$ Hz). The fit parameters (for a temperature of $T_{AC} + 0.2$) for a few selected points on the curves are given in Table I.

Fig. 15. Some of these differences found experimentally are listed below:

- In the SmC* phase, the birefringence saturates spontaneously for rather low values of the applied field, while in SmA* phase, the birefringence does not attain a complete saturation even for higher electric fields.
- The SmA* phase exhibits “U” shaped switching, whereas the SmC* phase exhibits “V” shaped one.
- We observe a prominent hysteresis in the SmC* phase, which is typical of a tilted smectic phase and this as well reflects optical bistability.

APPENDIX D: A SAMPLE DATASET FOR SELECTED POINTS OBTAINED FROM EXPERIMENTAL RESULTS

Table I given below lists the fit parameters that are selected for obtaining Δn using the ATP technique for a temperature of $T = T_{AC} + 0.2$.

APPENDIX E: THE DSC THERMOGRAM

The DSC thermogram of DRI33 under cooling is plotted in Fig. 16. The observed phase transition from SmA* to SmC* is a weak first-order. It may be pointed out that no discontinuity in the birefringence is observed at the SmA* to SmC* transition temperature possibly due to the reason that measurements are made on a rubbed planar-aligned cell of cell spacing $2 \mu\text{m}$. The surface effects are indeed very dominant. There is also a possibility of averaging out of the discontinuities due to the use of a non-monochromatic light source and finite size effects for measurements. This is in contrast to the

TABLE I. The fit parameters that are selected for obtaining Δn using the ATP technique for a temperature of $T = T_{AC} + 0.2$.

E ($\text{V}/\mu\text{m}$)	S_S	C_S	B_S	S_C	C_C	B_C	S_B	C_B	B_B	Δn
5.5	0.952	-0.353	0.003	-0.558	1.250	-0.013	0.002	-0.039	1.594	0.0604
10.5	1.056	-0.477	0.003	-0.630	0.974	-0.010	0.002	-0.041	1.584	0.0658
16.5	1.113	-0.512	0.002	-0.636	0.816	-0.008	0.001	-0.041	1.576	0.0688

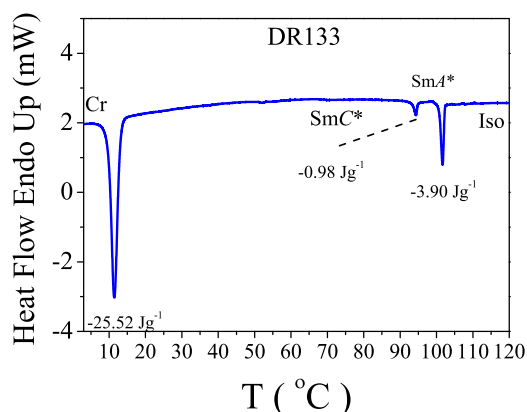


FIG. 16. The DSC thermogram of DR133 shown under cooling with a scan rate of 10 °C/min. The plot shows the transition enthalpies ($\Delta H/\text{Jg}^{-1}$) at the phase transitions. The Iso stands for the isotropic phase, and Cr denotes the crystalline state of the sample.

observations made of the birefringence where it discontinuously jumps at the first-order phase transitions in subphases of antiferroelectric liquid crystals⁴⁸ (See Figs. 4, 5, and 8 of Ref. 48). However in the latter case, the measurements are made on homeotropic aligned cells, of cell-thickness 50 μm . He-Ne laser is used as the source of light. For a homeotropic cell of 50 μm cell thickness the surface effects are negligibly small.

REFERENCES

- J. W. Goodby, P. J. Collings, T. Kato, C. Tschierske, H. F. Gleeson, and P. Raynes, *Handbook of Liquid Crystals* (Wiley VCH, 2014), Vol. 1.
- J. P. F. Lagerwall and F. Giesselmann, *Chem. Phys. Chem.* **7**, 20 (2006).
- Y. Takahashi, Y. Ouchi, H. Takezoe, and A. Fukuda, *Jpn. J. Appl. Phys.* **28**, L487 (1989).
- T. P. Rieker, N. A. Clark, G. S. Smith, D. S. Parmar, E. B. Sirota, and C. R. Safinya, *Phys. Rev. Lett.* **59**, 2658 (1987).
- S. Diele, P. Brand, and H. Sackmann, *Mol. Cryst. Liq. Cryst.* **16**, 105 (1972).
- A. de Vries, *Mol. Cryst. Liq. Cryst.* **41**, 27 (1977).
- A. J. Leadbetter and E. K. Norris, *Mol. Phys.* **38**, 669 (1979).
- A. de Vries, *Mol. Cryst. Liq. Cryst.* **49**, 179 (1979).
- A. de Vries, *J. Chem. Phys.* **71**, 25 (1979).
- A. de Vries, A. Ekachai, and N. Spielberg, *Mol. Cryst. Liq. Cryst.* **49**, 143 (1979).
- S.-I. Nishiyama, Y. Ouchi, H. Takezoe, and A. Fukuda, *Jap. J. App. Phys.* **26**, L1787 (1987).
- N. Kapernaum, D. M. Walba, E. Korblova, C. Zhu, C. Jones, Y. Shen, N. A. Clark, and F. Giesselmann, *Chem. Phys. Chem.* **10**, 890 (2009).
- Yu. P. Panarin, V. Panov, O. E. Kalinovskaya, and J. K. Vij, *J. Mater. Chem.* **9**, 2967 (1999).
- M. S. Spector, P. A. Heiney, J. Naciri, B. T. Weslowski, D. B. Holt, and R. Shashidhar, *Phys. Rev. E* **61**, 1579 (2000).
- J. P. F. Lagerwall, F. Giesselmann, and M. D. Radcliffe, *Phys. Rev. E* **66**, 031703 (2002).
- M. Skarabot, M. Cepic, B. Zeks, R. Blinc, G. Heppke, A. V. Kityk, and I. Musevic, *Phys. Rev. E* **58**, 575 (1998).
- C. C. Huang, S. T. Wang, X. F. Han, A. Cady, R. Pindak, W. Caliebe, K. Ema, K. Takekoshi, and H. Yao, *Phys. Rev. E* **69**, 041702 (2004).
- M. Skarabot, K. Kocevar, R. Blinc, G. Heppke, and I. Musevic, *Phys. Rev. E* **59**, R1323 (1999).
- C. V. Lobo, S. K. Prasad, and D. S. Rao, *Phys. Rev. E* **72**, 062701 (2005).
- U. Manna, J. K. Song, Yu. P. Panarin, A. Fukuda, and J. K. Vij, *Phys. Rev. E* **77**, 041707 (2008); V. Swaminathan, V. P. Panov, Yu. P. Panarin, S. P. Sreenilayam, J. K. Vij, A. Panov, D. Rodriguez-Lojo, P. J. Stevenson, and E. Gorecka, *Liq. Cryst.* **45**(4), 513–521 (2018).
- J. C. Roberts, N. Kapernaum, Q. Song, D. Nonnenmacher, K. Ayub, F. Giesselmann, and R. P. Lemieux, *J. Am. Chem. Soc.* **132**, 364 (2010).
- N. A. Clark, T. Bellini, R. Shao, D. Coleman, S. Bardou, D. R. Link, J. E. Maclennan, X. Chen, M. D. Wand, D. M. Walba, P. Rudquist, and S. T. Lagerwall, *Appl. Phys. Lett.* **80**, 4097 (2002).
- Y. Q. Shen, L. X. Wang, R. F. Shao, T. Gong, C. H. Zhu, H. Yang, J. E. Maclennan, D. M. Walba, and N. A. Clark, *Phys. Rev. E* **88**, 062504 (2013).
- M. V. Gorkunov, F. Giesselmann, J. P. F. Lagerwall, T. J. Sluckin, and M. A. Osipov, *Phys. Rev. E* **75**, 060701(R) (2007).
- M. V. Gorkunov and M. A. Osipov, *J. Phys.: Condens. Matter* **20**, 465101 (2008).
- S. T. Lagerwall, P. Rudquist, and F. Giesselmann, *Mol. Cryst. Liq. Cryst.* **510**, 1282 (2009).
- M. Osipov and G. Pająk, *Phys. Rev. E* **85**, 021701 (2012).
- D. M. Agra-Kooijman, H. Yoon, S. Dey, and S. Kumar, *Phys. Rev. E* **89**, 032506 (2014).
- S. Garoff and R. B. Meyer, *Phys. Rev. Lett.* **38**, 848 (1977); R. B. Meyer, L. Liebert, L. Strzelecki, and P. Keller, *J. Phys. Lett.* **36**, 69 (1975).
- J. V. Selinger, P. J. Collings, and R. Shashidhar, *Phys. Rev. E* **64**, 061705 (2001).
- S. P. Sreenilayam, D. Rodriguez-Lojo, V. P. Panov, V. Swaminathan, J. K. Vij, Yu. P. Panarin, E. Gorecka, A. Panov, and P. J. Stevenson, *Phys. Rev. E* **96**, 042701 (2017).
- S. P. Sreenilayam, D. M. Agra-Kooijman, V. P. Panov, V. Swaminathan, J. K. Vij, Yu. P. Panarin, A. Kocot, A. Panov, D. Rodriguez-Lojo, P. J. Stevenson, M. R. Fish, and S. Kumar, *Phys. Rev. E* **95**, 032701 (2017).
- M. J. Frisch et al., GAUSSIAN 09, Revision E.01, Gaussian, Inc., Wallingford, CT, 2009.
- B. Park, S. S. Seomun, M. Nakata, M. Takahashi, Y. Takahashi, K. Ishikawa, and H. Takezoe, *Jpn. J. Appl. Phys.* **38**, 1474 (1999).
- S. Huard, *Polarization of Light* (Wiley, 1997).
- P. G. de Gennes, *Physics of Liquid Crystal* (Clarendon Press, Oxford, 1974).
- W. H. de Jeu and P. Bordewijk, *J. Chem. Phys.* **68**, 109 (1978).
- E. G. Hanson and Y. R. Shen, *Mol. Cryst. Liq. Cryst.* **36**, 193 (1976).
- B. Zywicki, W. Kuczynski, and G. Czechowski, *Proc. SPIE* **2372**, 151 (1995).
- A. Marchetti, V. Domenici, V. Novotna, M. Lelli, M. Cifelli, A. Lesage, and C. A. Veracini, *Chem. Phys. Chem.* **11**, 1641 (2010).
- H. Yoon, D. M. Agra-Kooijman, K. Ayub, R. P. Lemieux, and S. Kumar, *Phys. Rev. Lett.* **106**, 087801 (2011).
- N. Hayashi, T. Kato, A. Fukuda, J. K. Vij, Y. P. Panarin, J. Naciri, R. Shashidhar, S. Kawada, and S. Kondoh, *Phys. Rev. E* **71**, 041705 (2005).
- N. Yadav, V. P. Panov, V. Swaminathan, S. P. Sreenilayam, J. K. Vij, T. S. Perova, R. Dhar, A. Panov, D. Rodriguez-Lojo, and P. J. Stevenson, *Phys. Rev. E* **95**, 062704 (2017); O. E. Panarina, Yu. P. Panarin, J. K. Vij, M. S. Spector, and R. Shashidhar, *Phys. Rev. E* **67**, 051709 (2003).
- A. Sanchez-Castillo, M. A. Osipov, S. Jagiella, Z. H. Nguyen, M. Kaspar, V. Hamplova, J. Maclennan, and F. Giesselmann, *Phys. Rev. E* **85**, 061703 (2012).
- A. Kocot, J. K. Vij, T. S. Perova, K. Merkel, V. Swaminathan, S. P. Sreenilayam, N. Yadav, V. P. Panov, P. J. Stevenson, A. Panov, and D. Rodriguez-Lojo, *J. Chem. Phys.* **147**, 094903 (2017).
- N. Hayashi, A. Kocot, M. J. Linehan, A. Fukuda, J. K. Vij, G. Heppke, J. Naciri, S. Kawada, and S. Kondoh, *Phys. Rev. E* **74**, 051706 (2006).
- V. Swaminathan, V. P. Panov, S. P. Sreenilayam, Yu. P. Panarin, and J. K. Vij, "A modified Langevin-Debye model for investigating the electro-optic behaviour of de Vries smectic liquid crystals," *Liquid Crystals* (published online 2018).
- A. D. L. Chandani, N. M. Shtykov, V. P. Panov, A. V. Emelyanenko, A. Fukuda, and J. K. Vij, *Phys. Rev. E* **72**, 041705 (2005).